Romanian Reports in Physics **72**, 119 (2020)

UNDERSTANDING GENERAL ROGUE WAVE SOLUTIONS OF THE GARDNER EQUATION

A. ANKIEWICZ[1,*], M. BOKAEEYAN[1], W. CHANG[2]

[1]Optical Sciences Group, Research School of Physics, The Australian National University, Canberra, ACT 2600, Australia

[*]Corresponding author, email: adrian.ankiewicz@anu.edu.au

[2]School of Electrical and Electronic Engineering, Nanyang Technological University, 639798, Singapore

Received July 3, 2020

Abstract. The Gardner equation is used as a generic model for internal waves and other phenomena. We find interesting structures revealed by rational solutions of this equation. We show the benefit of using the Hirota method to give simple forms, which are then used to generate the solutions. These forms are of lower order than the polynomials in the solutions themselves. Patterns and powers of these polynomials are discussed. A brief study of the poles of each solution elucidates the structure of various rogue wave solutions and allows us to gain understanding and insight regarding the features of such rogue waves. These solutions provided here have numerous applications in internal ocean waves and dusty-type plasmas.

Key words: Real-valued rogue waves, Rational solutions, Gardner equation, Bilinear Hirota method, Numerical analysis.

1. INTRODUCTION

In recent years, it has become apparent that rogue waves can explain numerous phenomena in science. The nonlinear focussing of energy can produce a high amplitude pulse or wave at a specific location. This can be useful in short-pulse measurements in physics and chemistry, but harmful in the ocean if a ship is hit by such a wave. There are various relevant reviews on the topic of rogue waves and related phenomena, applying to a range of physical settings [1–5].

The Gardner equation is a nonlinear partial differential equation named after C. Gardner who provided it in 1968 to generalize the Korteweg-de Vries (KdV) and modified KdV (mKdV) equations. It has been applied to studies in hydrodynamics (including internal waves) [6, 7], plasma physics [8, 9], undular bore theory [10], and solid-state physics [11]. Various works [11–15] have considered the Gardner equation. With unit coefficients, it is given by:

$$\psi_x + \psi\psi_t + \psi^2\psi_t + \psi_{ttt} = 0. \tag{1}$$

A recent paper [12], shows that its rational solutions can describe the evolution of

internal rogue waves in some three-layer fluids. Here, we employ the bilinear Hirota method to split the Gardner equation to two coupled equations for two unknown polynomials. We seek to find these low-order polynomials. These functions show up interesting patterns.

Equation (1) can support a wide range of solutions. A stationary soliton solution, as well as a new set of the rational solutions are among these. The latter ones predict rogue wave structures in internal waves [12] as well as in dusty plasma [9]. The first-order rational solution could be labelled a 'rational soliton solution' since it is stationary. However, from the second-order rational solution onwards, we find localized structures at the center (origin) of the waves.

Finding the first-order rational solution might be quite straightforward and can be obtained by direct substitution. However, determination of the higher-order solutions, including solitons, breathers, and rational solutions can be highly complicated and can require enormous computational time. In the case of rational solutions of the Gardner equation, it has been shown that they include bi-polynomials up to order 20 [12]. The explicit higher-order breather solutions of the Gardner equation [16] also include a myriad of exponential functions. Several useful techniques can be employed to find such complicated solutions. Each of those has its weaknesses and strengths. For example, a generalized Darboux transfromation has been used for finding the rational solutions of the mKdV equation [17]. The breather solutions of the Gardner equation have been also found using the inverse scattering transform by Pelinovsky and Grimshaw [18]. The interaction between solitons and breathers has also been obtained using the bilinear Hirota method for the fixed coefficients [16] and for variable coefficients [19]. The latter technique simplifies the procedure by splitting the original equation into two separate equations. The lack of complexity involved in the latter approach compared with the other approaches makes it applicable and appropriate for the KdV family of the equations. In this paper, we will employ this technique to find rational solutions of the Gardner equation (1) and show that these solutions can be obtained in a simplified way.

In order to be an applicable solution, a rational solution should have no singularities. In other words, the denominator of the solution should only possess complex zeros with non-zero imaginary part. Residues at these zeros are strongly dependent on the poles. Recently, in our previous work [20] we showed that, surprisingly, the residues for the rational solution poles of the Gardner equation add to give integer values. Furthermore, integral relations that characterize the Gardner rogue waves were presented, and it was shown that they also take integer values. These could be used to identify the order of a measured rogue wave from experimental results.

It has been unclear how the poles of the rational solutions of evolution equations can delineate the dynamics of the solutions themselves. Studying the poles to illustrate the localized structures has not been emphasized in the theory of nonlin-

ear waves in the past. Nevertheless, some previous works in the theory of solitons and stationary solutions should be highlighted. For example, an approach based on the dynamics of the poles was successfully adopted to help in the understanding of collisions of solitons and their interactions for the Korteweg-de Vries equation.

Poles can be useful for identifying the invariant quantities for rational solutions. Poles of the rogue wave solutions of the nonlinear Schrödinger (NLS) equation were used to find some conserved quantities [21]. Their manifestation is more than artistic, since their dynamics can be useful in describing the localized peaks. It has been shown [22] that the location of poles in the complex plane correlates with the localized maxima or minima in the Boussinesq equation [23]. Furthermore, the location of maximum displacements of these rogue waves defined by the NLS equation corresponds to the movement of poles of the exact solutions [24]. This can be exact for the first-order rogue wave; however, numerical analysis was needed to show it for the second-order solution.

To extend to the second-order rational solution, the locations of second-order rogue waves are shown to correlate with the movement of poles in the complex plane, if the spatial variable of the exact solution is extended by analytic continuation. More recently, it has been found that the imaginary parts of the coordinates of the poles of the rogue wave solutions will correlate with the amplitudes at the points of maximum displacement in the physical space. The focus is then on point(s) where the variations of the imaginary parts of the pole trajectories reverse directions in the complex plane. In particular, a smaller magnitude of the imaginary part of the coordinate of the pole will typically be associated physically with a region of larger amplitude of the rogue wave.

In a later part of the paper, we will show that the dynamics of the poles can be useful in the study of the dynamics of rogue wave solutions of the Gardner equation. The poles are linked to the eigenvalues of the solution. Moreover, a footprint of the rogue waves can be found using the real part of poles at which the imaginary part is minimum.

2. PRINCIPLES

We consider the Gardner equation in the form:

$$\psi_x + \psi\psi_t + 6\psi^2\psi_t + \psi_{ttt} = 0. \tag{2}$$

If we have a solution of Eq. (1), then we can obtain the corresponding solution of Eq. (2) by using $\psi \to \psi/6, t \to t/\sqrt{6}, x \to x/(6\sqrt{6})$.

A direct derivation of the Hirota equations for the KdV equation can be found

in [25]. We set $\psi = G/F$. We find:

$$F^2(D_x + D_t^3)G \diamond F + (D_t G \diamond F)\,[G(6G+F) - 3(D_t^2 F \diamond F)] = 0. \tag{3}$$

Here the Hirota operator D_z^n is:

$$D_z^n F \diamond G = (\frac{\partial}{\partial z} - \frac{\partial}{\partial z'})^n G(x,t)F(x',t'),$$

where z can be x or t. Now suppose that the term in square brackets is λF^2. This is an assumption, based on partial knowledge of the desired solutions, which restricts the possible range of the solutions. Here, λ an arbitrary constant parameter or function that has been introduced. In this case, we obtain the two coupled Hirota bilinear equations:

$$(D_x + D_t^3)G \diamond F + \lambda D_t G \diamond F = 0, \tag{4}$$

and

$$3(D_t^2 F \diamond F) - G(6G+F) = \lambda F^2. \tag{5}$$

The system of equations, Eqs. (3) and (5), can be written as:

$$G_x F - F_x G + G_{ttt}F + 3G_{tt}F_t + 3G_t F_{tt} - GF_{ttt}$$

$$+\lambda(G_t F - F_t G) = 0. \tag{6}$$

$$6(F_{tt}F - F_t^2) - G(6G+F) = -\lambda F^2. \tag{7}$$

Henceforth, we take λ to be zero. Therefore, we expect the solutions to take the forms:

$$\psi_n(x,t) = 2[\arctan(\frac{g(x,t)}{f(x,t)})]_t = -2[\arctan(\frac{f(x,t)}{g(x,t)})]_t$$

$$= \frac{1}{i}\big[\ln\left(-1 + \frac{2f(x,t)}{f(x,t) - ig(x,t)}\right)\big]_t. \tag{8}$$

The benefit is that $g(x,t)$ and $f(x,t)$ are lower order, and thus easier to handle, than the polynomials appearing in ψ_n found in our earlier paper [12]. Note that, from the definition,

$$\psi_n = 2\frac{f(x,t)g_t(x,t) - f_t(x,t)g(x,t)}{f^2(x,t) + g^2(x,t)}$$

$$= 2\frac{D_t(g \diamond f)}{f^2(x,t) + g^2(x,t)},$$

where $D_t(g \diamond f)$ is the Hirota bilinear derivative explained above. This shows that the solutions will be non-singular, since f and g are real-valued functions. For a given order, n, suitable functions $f = f_n$ and $g = g_n$ can be sought. In order to get

some insight into the structure of these rogue wave solutions, we consider the forms of f and g needed to give the simplest results.

Thus, if we write $\psi_n = u_t$, then

$$u = 2\arctan(\frac{g(x,t)}{f(x,t)}).$$

We can integrate Eq. (2) to give

$$J[u] = u_x + \frac{1}{2}u_t^2 + 2u_t^3 + u_{ttt} = constant, \tag{9}$$

and we take this constant to be zero. Substituting in u, we find that:

$$\frac{1}{2}[f^2(x,t) + g^2(x,t)]^2 J[u] = (f_t g - g_t f) J_1 + [f^2(x,t) + g^2(x,t)] J_2 = 0, \tag{10}$$

where

$$J_1 = 6(f_{tt}f - f_t^2 + g_{tt}g - g_t^2) - (g_t f - f_t g), \tag{11}$$

and

$$J_2 = g_x f - f_x g + g_{ttt}f - 3g_{tt}f_t + 3g_t f_{tt} - g f_{ttt}. \tag{12}$$

We now choose to set $J_1 = 0$ and $J_2 = 0$ separately, in analogy with the formation of the Hirota bilinear equations given above for the larger polynomials G and F. For the various orders, we now seek low order polynomials f and g to satisfy Eqs. (11) and (12).

3. ANALYSIS OF FUNCTIONS

We now need to specify the forms for $g(x,t)$ and $f(x,t)$ used in deriving the n^{th} order rogue wave. We set

$$g_n = \sum_{j=0}^{n-1} h_j^{[n]}(t) x^j,$$

$$f_n = \sum_{j=0}^{n-1} s_j^{[n]}(t) x^j. \tag{13}$$

We set the leading order coefficient to be positive.

3.1. FUNCTIONS FOR FIRST ORDER

For the 1st order, we can set one of the functions to be constant and set the other one to be independent of the variable x. It is straightforward to show that:

$$\begin{aligned} g_1 &= h_0^{[1]} = 6, \qquad (14)\\ f_1 &= s_0^{[1]}(t) = t. \end{aligned}$$

$$(15)$$

Thus, $h_0^{[1]} = 6 s_0^{[1]\prime}(t)$. Similar relations (patterns) will appear later for the higher-order sub-polynomials. From the above, we find the known soliton-like form:

$$\psi_1 = -\frac{12}{t^2+36}. \qquad (16)$$

This solution is a stationary solution for the Gardner equation, as it does not depend on the evolution value x.

3.2. FUNCTIONS FOR SECOND ORDER

For the second order, we set one of the functions of $f(x,t)$ and $g(x,t)$ to be independent of the propagation axis, viz. x, and the other one to be a linear function with respect to x. Hence for second order, we can write:

$$g_2(x,t) = h_0^{[2]}(t),$$

$$f_2(x,t) = s_0^{[2]}(t) + x s_1^{[2]}.$$

It is easy to show that:

$$\begin{aligned} s_0^{[2]}(t) &= t\left(t^2 - 108\right), \qquad (17)\\ s_1^{[2]} &= 12,\\ h_0^{[2]}(t) &= 18\left(t^2+36\right). \end{aligned}$$

Thus,

$$s_1^{[2]}(t) = 2 s_0^{[2]\prime\prime\prime}(t) = 12. \qquad (18)$$

Further

$$h_0^{[2]}(t) - 6 s_0^{[2]\prime}(t) = 1296. \qquad (19)$$

Then

$$h_0^{[2]\prime}(t) = 6 s_0^{[2]\prime\prime}(t) = 36t. \qquad (20)$$

So

$$\psi_2 = -\frac{36(t^4 + 216t^2 - 24tx - 3888)}{t^6 + 108t^4 + 24t^3x + 34992t^2 - 2592tx + 144(x^2+2916)}. \qquad (21)$$

Taking this as $\psi_2(x,t) = G/F$ it is easy to verify that G and F satisfy Eqs. (6) and (7) with $\lambda = 0$.

As noted above, the benefit is that g and f are lower order than the polynomials in ψ_2. Here $f_t = 3t^2 - 108$ and $g_t = 36t$. Thus, above, the denominator in Eq. (21) is equal to $(t^3 - 108t + 12x)^2 + [18(36 + t^2)]^2$. This corresponds to the form given in [12].

3.3. FUNCTIONS FOR THIRD ORDER

A similar scenario can be followed to find the patterns of the third- and fourth-order sub-functions. Following Eq. (13) for the 3rd order, we can write:

$$g_3 = h_0^{[3]}(t) + h_1^{[3]}(t)x$$

$$f_3 = s_0^{[3]}(t) + s_1^{[3]}(t)x + s_2^{[3]}x^2.$$

After some algebraic calculations, we will find:

$$\begin{aligned} s_0^{[3]}(t) &= \frac{t^6}{720} - \frac{3t^4}{4} - 81t^2 - 2916, \\ s_1^{[3]}(t) &= \frac{1}{12}t\left(t^2 - 108\right) = \frac{1}{2}s_0^{[3]\prime\prime\prime}(t), \\ h_0^{[3]}(t) &= t\left(\frac{t^4}{20} + 972\right), \\ h_1^{[3]}(t) &= \frac{3}{2}\left(t^2 - 108\right), \end{aligned} \tag{22}$$

where $s_2^{[3]} = -1$ is a constant only. We note that the polynomials have positive terms of highest order.

We find that there are simple relations between these polynomials. For example,

$$s_0^{[3]\prime\prime\prime}(t) = 2s_1^{[3]}(t), \tag{23}$$

and

$$h_0^{[3]}(t) - 6s_0^{[3]\prime}(t) = 18t(t^2 + 108), \tag{24}$$

while

$$h_1^{[3]}(t) = 6\,s_1^{[3]\prime}(t) - 108. \tag{25}$$

Also $18s_1^{[3]}(t) = t\,h_1^{[3]}(t)$, while $h_0^{[3]\prime\prime\prime}(t) - 2h_1^{[3]}(t) = 324$.

Using the 'arctan' expression, we now find $\psi_3 = G_3/D_3$. Then:

$$G_3 = -72[t^{10} + 540t^8 + 272160t^6 - 25920t^5x$$

$$+5400t^4\left(x^2 - 3888\right) + 9331200t^3x - 388800t^2\left(x^2 + 2916\right)$$

$$+43200tx\left(x^2+11664\right)+6998400\left(5x^2+5832\right)].$$

Then

$$\begin{aligned} D_3 =& t^{12}+216t^{10}+120t^9x+174960t^8 \\ &+2160t^6\left(x^2+50544\right)-8398080t^5x \\ &+1166400t^4\left(x^2+4860\right)-86400t^3x\left(x^2-23328\right) \\ &-125971200t^2\left(x^2-5832\right)+9331200tx\left(x^2-14580\right) \\ &+518400\left(x^4+32076x^2+8503056\right). \end{aligned} \tag{26}$$

The coefficients differ from those in [12] because a factor of 6 has been put into the equation in this paper, and it was unity in [12].

It is straightforward to show that this satisfies the Gardner equation, *i.e.* Eq. (2).

Table 1

Highest powers in polynomials in t characterizing rogue waves of the Gardner equation. For the x^0 terms, *i.e.* those in which x does not appear, this is the triangle number $n(n+1)/2$ [26] for $s_0(t)$ that appears in f_n, and is $n(n+1)/2-1$ for $h_0(t)$ that appears in g_n. This uses results given in equations 14, 17, 22, and 27.

n	$h_0^{[n]}(t)x^0$	$s_0^{[n]}(t)x^0$	$h_1^{[n]}(t)x^1$	$s_1^{[n]}(t)x^1$	$h_2^{[n]}(t)x^2$	$s_2^{[n]}(t)x^2$
1	0	1	0	0	0	0
2	2	3	0	0	0	0
3	5	6	2	3	0	0
4	9	10	6	7	0	1

3.4. FUNCTIONS FOR 4TH ORDER

We now need to extend the $ansatz$ for g_4 and f_4:

$$\begin{aligned} g_4 &= h_0^{[4]}(t)+xh_1^{[4]}(t)+x^2h_2^{[4]}(t)+x^3h_3^{[4]}, \\ f_4 &= s_0^{[4]}(t)+xs_1^{[4]}(t)+x^2s_2^{[4]}+x^3s_3^{[4]}(t). \end{aligned} \tag{27}$$

Now, we find:

$$h_0^{[4]}(t)=60t\left[t^8-216t^6+29393280(t^2-54)\right],$$

$$s_0^{[4]}(t)=t^{10}-1620t^8-272160t^6-146966400(1944+162t^2+t^4),$$

while

$$h_1^{[4]}(t)=7560\left[t^6-180t^4+58320(84-t^2)\right],$$

$$s_1^{[4]}(t) = 180t\left[t^6 - 756t^4 + 45360(108 + t^2)\right].$$

Then $h_2^{[4]}(t) = 65318400t$ and $s_2^{[4]} = -391910400$, and $h_3^{[4]} = 1814400$ and $s_3^{[4]}(t) = 302400t$. Thus $h_2^{[4]}/s_2^{[4]} = -(t/6)$, while $h_2^{[4]}(t)/h_3^{[4]}(t) = 36t$ and $h_2^{[4]} = 216s_3^{[4]}$.

So

$$\frac{s_0^{[4]\prime\prime\prime}(t) - 4s_1^{[4]}(t)}{h_2^{[4]}(t)} = -(t^2 + 108). \tag{28}$$

This is analogous with Eqs. (18) and (23). Also $s_0^{[4]\prime\prime\prime}(t) + 4s_1^{[4]}(t) = 1440t^5\left(t^2 - 756\right)$.

Then

$$\frac{h_1^{[4]}(t) - 6s_1^{[4]\prime}(t)}{h_3^{[4]}(t)} = \frac{3}{2}(t^2 - 108)^2. \tag{29}$$

This is analogous with Eqs. (19) and (24). With these functions, g_4, f_4 satisfy Eqs. (11) and (12).

The resulting

$$\psi_4(x,t) = 2[\arctan(\frac{g_4(x,t)}{f_4(x,t)})]_t \tag{30}$$

satisfies the Gardner equation, *i.e.* Eq. (2).

Table 2

The rogue wave is given by $\psi_n = G_n/D_n$. The columns give the total number of terms occurring in G_n, D_n, g_n, and f_n, respectively. Plainly far fewer terms appear in g_n and f_n, showing the convenience of this approach. This uses results given in equations 16, 21, 26, and 30 for G_n, D_n , as well as the functions g_n and f_n given in equations 14, 17, 22, and 27.

n	G_n	D_n	g_n	f_n
1	1	2	1	1
2	4	7	2	3
3	13	18	4	7
4	33	39	10	12

3.5. POLYNOMIALS: EVEN AND ODD

By looking at these functions for various orders, we observe some patterns by using results given in equations 14, 17, 22, and 27. These are listed in Table 1.

The columns in Table 2 give the total number of terms occurring in G_n, D_n, g_n, and f_n, respectively. Plainly far fewer terms appear in f and g, showing the benefit of this approach.

When the highest power in t in $h_j^{[n]}(t)$ is even, then the whole polynomial $h_j^{[n]}(t)$ is even. When the highest power in t in $h_j^{[n]}(t)$ is odd, then the whole polyno-

mial $h_j^{[n]}(t)$ is odd. For example, in the 3rd order example of the previous Section, Eq. (22), $h_0^{[3]}(t)$ and $s_1^{[3]}(t)$ are fully odd, while $h_1^{[3]}(t)$ and $s_0^{[3]}(t)$ are fully even. This can reveal the inversion-reflection symmetry, as an important feature, for the solutions of the Gardner equation. If we use the general polynomials for these functions, then we can import arbitrary parameters, which can show the dynamics for these waves.

The four lowest order Gardner rogues all have zero background in the formulation here. The centre values for $n = 1,2,3,4$ are respectively $-\frac{1}{3}, \frac{1}{3}, -\frac{2}{3}, \frac{2}{3}$. So, in terms of earlier notation, $n = 1,3$ forms are 'dark', while $n = 2,4$ forms are 'bright'. The extrema take values one-sixth of those found with the other normalization [12].

4. COMPARISON WITH MKDV FUNCTIONS

The mKdV equation is:

$$\psi_x + 6\psi_t\psi^2 + \psi_{ttt} = 0. \tag{31}$$

We now make a comparison with functions needed to provide the mKdV rogue waves. Here the solution of order n is given by $\psi = \psi_n(x,t)$, where

$$\psi_n(x,t) = 2[\arctan(\frac{g(x,t)}{f(x,t)})]_t + (-1)^n.$$

The denominator is $f^2 + g^2$ and f and g are real functions, so the solutions are clearly non-singular. We can also write the solutions in the form:

$$\psi_n(x,t) = \frac{G_n}{D_n} + (-1)^n.$$

The max value is $2n+1$ and this occurs at the origin [27].

For $n = 1$, we have $g = 1$ and $f = -2(t - 6x)$. Hence

$$\psi_1(x,t) = \frac{4}{4(t-6x)^2+1} - 1. \tag{32}$$

For $n = 2$, we have

$$g = 3\left[4(t-6x)^2 + 1\right]$$

and

$$f = 8(t-6x)^3 - 6(t-22x).$$

Hence

$$G_2(x,t) = 6\{6 - 16(t-6x)[2t^3 - 36t^2x + 3t\left(72x^2+1\right) - 6x\left(72x^2+11\right)]\}.$$

while

$$D_2(x,t) = 9\left[4(t-6x)^2+1\right]^2 + \left[6(t-22x) - 8(t-6x)^3\right]^2.$$

Moving to $n = 3$, we have

$$g = -12\left[16(t-6x)^5 + 480x(t-6x)^2 + 15(t-6x) - 360x\right]$$

and

$$f = 64(t-6x)^6 - 240(t-6x)^4 + 3840x(t-6x)^3 - 180(t-6x)^2 \\ -2880x(t-6x) - 46080x^2 - 45.$$

We have

$$G_3 = -24[-1024(t-6x)^{10} - 3840(t-6x)^8 - 13440(t-6x)^6 \\ + 7200(t-6x)^4 + 2700(t-6x)^2 + \cdots],$$

so it is clear that, in each case, the functions f and g are of much lower order, and are thus easier to handle.

5. GENERALIZED FORMS FOR LOWEST ORDER RATIONAL SOLUTIONS

We now consider a generalized form of the equation. We set:

$$\psi_x + 6\psi\psi_t(k + m\psi) + \psi_{ttt} = 0, \tag{33}$$

where k and m are real constants. So, when $k = 1/6, m = 1$ this reduces to Eq. (2) from near the beginning of this paper. While, if $k = 1/6, m = 1/6$, it reduces to Eq. (1) from the beginning of this paper. Also when $k = 0$ and $m = 1$, this reduces to Eq. (31) of the previous Section. Lastly, if we set $k = -1$ and $m = 0$, it reduces to the KdV equation we studied relating to shallow water waves [28]:

$$\psi_x - 6\psi\psi_t + \psi_{ttt} = 0, \tag{34}$$

When $m = 0$, for any $k \neq 0$, we set $j = 2(6kx + t) + i\,c$ and use

$$\psi = \frac{2}{k}(\ln j)_{tt} - 1$$

to get

$$\psi = -1 - \frac{8}{k[2(6kx + t) + i\,c]^2}, \tag{35}$$

for $c \neq 0$. For $k = -1$, this reduces to the form found in [28].

For the rest of this Section, we use:

$$\psi(x,t) = \frac{2}{\sqrt{m}}[\arctan(\frac{g(x,t)}{f(x,t)})]_t - 1, \tag{36}$$

with $m \neq 0$. When $k = 1/6$, for any $m \neq 0$, we have $f = c_0 + \left(\frac{1}{6} - 2m\right)(-6mx + t + x)$ and $g = \sqrt{m}$, where c_0 is an arbitrary constant. Setting it to zero and using Eq.

(36) for the case $m = 1$ gives

$$\psi = \frac{132}{121(t-5x)^2+36} - 1,$$

which is a form of the solution of Eq. (16) with non-zero velocity (*i.e.* tilt).

Now, for $k = 0$ with any $m \neq 0$, we have:

$$\psi = \frac{4}{4m(t-6mx)^2+1} - 1.$$

Clearly, the $m = 1$ form of this gives the mKdV result of the previous Section, viz. Eq. (32).

For general k, m with $m \neq 0$, we have $f = c_1 + (k-2m)[6x(k-m)+t]$, while $g = \sqrt{m}$. Here, $c_1 = ick/2$ is an arbitrary constant. We set it to zero here for simplicity. Hence

$$\psi = \frac{2(2m-k)}{m+B^2(k-2m)^2} - 1,$$

where $B = 6x(k-m)+t$. In fact, this form is still valid when $m = 0$. It then reduces to $\psi = -1 - \frac{8}{k[2(6kx+t)+ic]^2}$, which matches Eq. (35).

6. GENERALIZED FORMS FOR SECOND-ORDER RATIONAL (ROGUE) SOLUTIONS

We now find the second-order solutions for Eq. (33). First we set $k = 1/6$ and allow m to be arbitrary. We find

$$g = h_0(t),$$

$$f = s_0(t) + xs_1$$

as before, where

$$\begin{aligned} s_0(t) &= \sqrt{m}\, t\left(t^2 - 108m\right), \\ s_1 &= 12\sqrt{m}, \\ h_0(t) &= 18m\left(t^2 + 36m\right). \end{aligned} \tag{37}$$

So, using

$$\psi(x,t) = \frac{2}{\sqrt{m}}[\arctan(\frac{g(x,t)}{f(x,t)})]_t, \tag{38}$$

we find:

$$\psi_2 = \frac{36\left(3888m^2 - 216mt^2 - t^4 + 24tx\right)}{9(36m)^3 + 27(36mt)^2 + 108m\left(t^4 - 24tx\right) + \left(t^3 + 12x\right)^2}.$$

We now allow k to be arbitrary, as well. Now

$$\begin{aligned} s_0(t) &= 216k\sqrt{m}t\left(k^2t^2-3m\right), \\ s_1 &= 12(6k)^3\sqrt{m}, \\ h_0(t) &= 648m\left(k^2t^2+m\right). \end{aligned} \tag{39}$$

If $k=1/6$, these reduce to Eq. (37) above. So, using Eq. (38), we find:

$$\psi_2 = -\frac{6k\left(k^4t\left(t^3-24x\right)+6k^2mt^2-3m^2\right)}{k^6\left(t^3+12x\right)^2+3k^4mt\left(t^3-24x\right)+27k^2m^2t^2+9m^3}.$$

For $k=1/6, m=1$ these reduce to the results given in Eqs. (17) and (21). For the KdV alone ($m=0$, any k), we have: $\psi_2 = \frac{2}{k}\left(\ln j_2\right)_{tt} - 1$ where

$$j_2 = 3\left[c_p - 4k(6kx+t)^2\right] + 8k^{3/2}(6kx+t)^3 + 6\sqrt{k}(22kx+t),$$

with c_p being a non-zero complex constant. When $k=-1$, this reduces to the form given in [28].

7. GENERALIZED FORM FOR THE SOLUTIONS

Now, if the functions f and g include more terms, of both odd and even powers, it will allow us to derive solutions with one or more free parameters. The Hirota method simplifies the calculation and requires us to find two 'simple' functions; this makes calculations easier and fairly straightforward. Here, we will now demonstrate this for the second-order solution. It is quite straightforward to show that the second-order solution can be found from these two general polynomials:

$$g(x,t) = 2\left[\alpha_1^2+6\alpha_1 t+9\left(t^2+36\right)\right],$$

$$f(x,t) = \left[t^3+\alpha_1 t^2+\frac{1}{3}\left(\alpha_1^2-324\right)t+\alpha_2\right]+12x,$$

where α_1 and α_2 are real free parameters. Here, f and g satisfy $J_1=0$ and $J_2=0$ from Eqs. (11) and (12). If α_1 and $\alpha_2 \to 0$, then the original forms, Eqs. (17) and (18), are retrieved. This leads to $\psi_2 = A/B$, where

$$A = -12\left[(\alpha_1+3t)\left(\alpha_1^3+3\alpha_1^2t+9\alpha_1t^2+9A_1\right)-104976\right],$$

and

$$\begin{aligned} B = \alpha_1^4\left(t^2+36\right)+6\alpha_1^3t\left(t^2+72\right)+3\alpha_1^2\left(tB_1+7776\right) \\ +18\alpha_1t\left(tB_2+7776\right)+9\left[\alpha_2^2+24x\left(\alpha_2+t^3-108t\right)+B_3\right], \end{aligned}$$

where $A_1 = -2\alpha_2+t^3+216t-24x$, $B_1 = \left(2\alpha_2+5t^3+432t+24x\right)$, while $B_2 = \left(\alpha_2+t^3+108t+12x\right)$ and $B_3 = 2\alpha_2t^3-216\alpha_2t+t^6+108t^4+34992t^2+144x^2+419904$.

This generalizes Eq. (21).

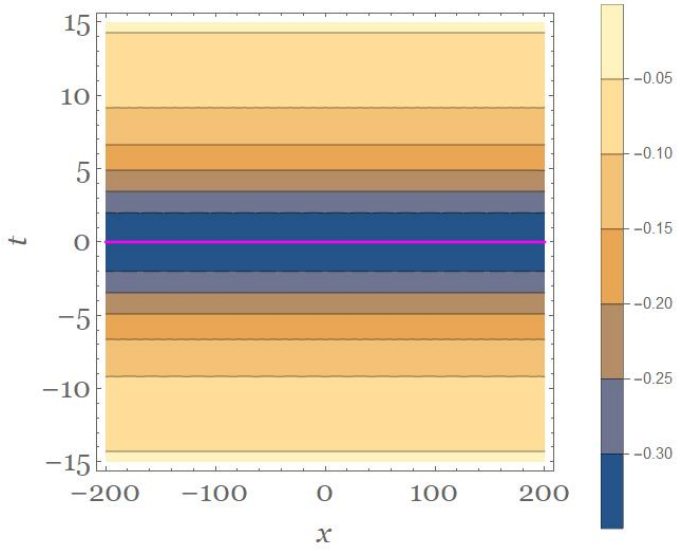

Fig. 1 – (Colour online) Contour plot of the first-order rational solution, Eq. (16). Here, there is only one complex pair of poles, $t = \pm 6i$, and the pink line here gives its real part as the ridge line, $t = 0$. This is valid for all x.

8. RELATING POLES TO ROGUE WAVE RIDGES

It has been conjectured that the location of the maximum height of a rogue wave for some value of its evolution variable (x) occurs at the real part of a pole, where the pole of the exact solution has the minimum absolute imaginary part, *i.e.* it is smaller than for the other poles [29]. For the Boussinesq equation, it has been shown in [22] that the rogue wave in that case, for a given x (propagation direction) value, tends to have maxima near t values where complex roots of the function of the denominator (F) have imaginary parts of minimal absolute values. We seek to investigate a related phenomenon here for the Gardner equation.

8.1. POLES AND BILINEAR FUNCTIONS

Thus, the objective here is to apply this scheme of pole movements to the dynamics of the Gardner rogue waves. In particular, this approach can provide particular relations between the maxima of the rogue wave profiles in the physical plane and the real parts of the poles in the extended complex plane. This approach has been applied to the Boussinesq and the NLS equations, but this could be valid for other evolution equations like the Gardner, mKdV or even the complex-valued KdV equation, and we investigate this. We firstly consider the rational quasi-soliton solution

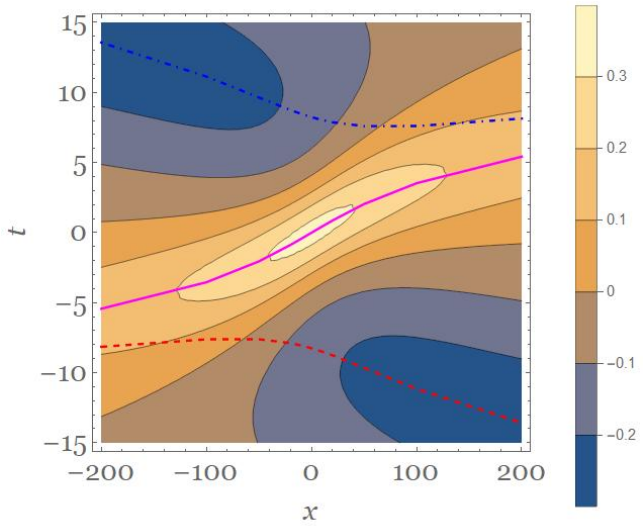

Fig. 2 – (Colour online) Contour plot of the second-order rogue wave, eqn.(21). Onto these level contours, we superimpose plots of the real parts of all of complex zeroes of the function denominator. There are three complex conjugate pairs, so three curves appear here, and they are included with the contour plot for this second-order rogue wave. Clearly, following the central (continuous pink) curve closely gives the positive ridge, while the upper (blue dot-dashed) one and lower (red dashed) ones hardly affect it. These latter curves appear to largely specify the positions of the function's minima (at upper left and lower right) of the rogue wave.

of the Gardner equation of Sec. (3.1). We then extend this idea to the second-order [Sec. (3.2)] and third-order [Sec. (3.3)] rational solutions.

8.2. RATIONAL SOLITON

By looking at the denominator of the first-order rational solution derived in Section (3.1), viz. equation (16), it can easily be found that the two poles are placed at $t = 6i$ and $t = -6i$.

Thus,

$$\psi_1(x,t) = i\left(\frac{1}{t-6i} - \frac{1}{t+6i}\right), \tag{40}$$

so the poles occur at $\xi_1(x) = 6i$ and $\xi_2(x) = -6i = \xi_1^*(x)$. Hence

$$\psi_1 = -\frac{12}{t^2+36}, \tag{41}$$

thus agreeing with Eq. (16). The real parts of these two poles occur at $t = 0$. Figure 1 has been plotted for the first-order rational solution. A constant velocity could be added to the form of equation (16) through the Gardner transformation given in [12].

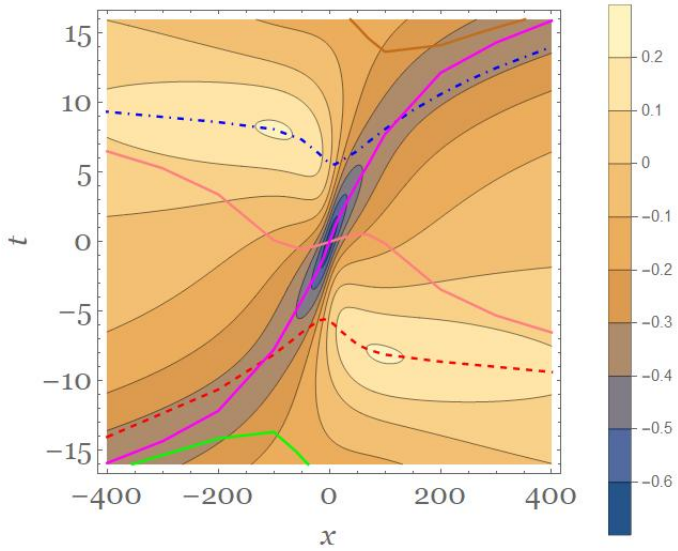

Fig. 3 – (Colour online) Contour plot of the third-order rogue wave, Eq. (26). Onto these level contours, we superimpose plots of the real parts of all of the complex (conjugate) zeroes of the function denominator. There are six complex conjugate pairs, so six curves appear here, and they are added to the contour plot for this third-order rogue wave. Clearly, following the central (pink) curve, going from lower left to upper right, closely gives the positive ridge over much of the range, while the other zeros hardly affect it.

The ridge occurs on the line $t = 0$ as there is only one complex pair of zeroes of $t^2 + 36$ in this case.

8.3. HIGHER-ORDER RATIONAL SOLUTIONS

We study the real parts of the poles at which the imaginary parts tend to be minimized. In Fig. 2, we plot the second-order rogue wave by indicating its contours. The three coloured lines show the real parts of the poles of the function (*i.e.* zeros of the denominator) over a range of x values. The pink curve, going from lower left to upper right, and including the origin, is the one with smallest imaginary part over the whole x range shown in Fig. 2. Plainly this curve follows the main positive ridge. However, this is not the case when $|x|$ exceeds around 250. In that case, the red (dashed) and blue (dot-dashed) curves indicate the deep 'valley' regions (in dark colours) on the upper left and lower right. Then, the blue (dot-dashed) curve indicates an upper left extremum (minimum) of the function, while the red (dashed) curve indicates a lower right extremum (minimum) of the function. So tracking these poles signifies the presence of local extrema.

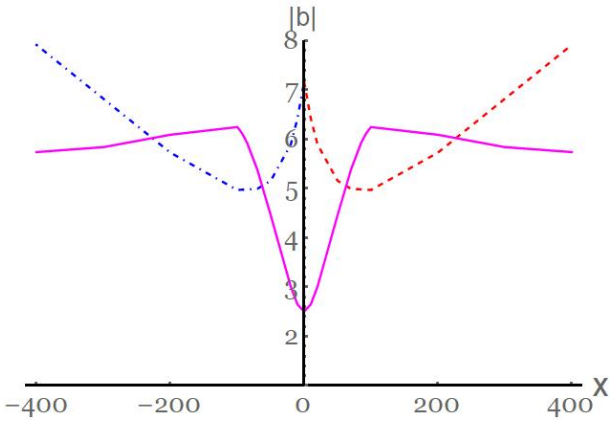

Fig. 4 – Plot of absolute value of the imaginary part, $|b|$, of three of the pairs of complex conjugate zeroes of the function denominator for the third-order rogue wave. The pink curve only has minimum absolute imaginary part for $|x| \lesssim 70$ and $|x| \gtrsim 225$, so this criterion is only suggestive and does not fully specify the ridge. For $70 \lesssim x \lesssim 225$, the red dashed curve has the minimum absolute imaginary part, while for $-225 \lesssim x \lesssim -70$, the blue dot-dash curve has the minimum absolute imaginary part.

In Fig. 3, we plot the third-order rogue wave, also by indicating its contours. The six coloured lines plotted on top of these contours show the real parts of the poles of the function (*i.e.* zeros of the denominator) over a range of x values. The pink curve, going through the origin, is the one with smallest imaginary part over only a part of the x range shown in Fig. 3. Plainly this curve follows the central extremum, which is a 'valley' in this case.

To investigate this more closely, in Fig. 4, we plot imaginary parts of three of the poles. So, for a given x, if the denominator has a zero at $t = a + ib$, then the function has a pole at this value of t. We plot $|b|$ in each case. The curve colours correspond to those used in Fig. 3. For $70 \lesssim x \lesssim 225$, the red (dot-dashed) curve has the minimum absolute imaginary part, and this explains the 'hill' region on the lower right of Fig. 3. For $-225 \lesssim x \lesssim -70$, the blue (dot-dashed) curve has the minimum absolute imaginary part, and this explains the 'hill' region on the upper left. The red (dashed) curve is only plotted for positive x. This curve exhibits the minimum absolute value of imaginary part near the point $(x = 100, t = -8)$ where the rogue wave attains its equal maximum (positive) value. The blue (dot-dashed) curve is only plotted for negative x. It exhibits the minimum absolute value of imaginary part near the point $(x = -100, t = +8)$ where the rogue wave attains its equal maximum value. The pink (continuous) curve is plotted for all x. This curve follows the valley where the rogue wave exhibits its minimum value. This, in fact, is the maximum *absolute* value of the function. As noted earlier, the pink (continuous) curve does not have the minimum absolute value of imaginary part over the whole range.

9. CONCLUSIONS

We have used the Hirota bilinear method to obtain the rogue waves of the Gardner equation. This procedure allows the use of polynomials that are of lower order than the functions appearing in the final forms. We showed that the poles of a solution provide information about the shape of the function itself and the position of its ridge.

REFERENCES

1. M. Onorato, S. Residori, U. Bortolozzo, A. Montina, and F. T. Arecchi, Rogue waves and their generating mechanisms in different physical contexts, Phys. Rep. **528**, 47–89 (2013).
2. N. Akhmediev *et al.*, Roadmap on optical rogue waves and extreme events, J. Opt. **18**, 063001 (2016).
3. S. Chen, F. Baronio, J. M. Soto-Crespo, Ph. Grelu, and D. Mihalache, Versatile rogue waves in scalar, vector, and multidimensional nonlinear systems, J. Phys. A: Math. Theor. **50**, 463001 (2017).
4. B. A. Malomed and D. Mihalache, Nonlinear waves in optical and matter-wave media: A topical survey of recent theoretical and experimental results, Rom. J. Phys. **64**, 106 (2019).
5. Y. Song, Z. Wang, C. Wang, K. Panajotov, and H. Zhang, Recent progress on optical rogue waves in fiber lasers: status, challenges, and perspectives, Advanced Photonics **2** (2), 024001 (2020).
6. T. G. Talipova, O. E. Kurkina, E. A. Rouvinskaya, and E. N. Pelinovsky, Propagation of solitary internal waves in two-layer ocean of variable depth, Izvestiya, Atmospheric and Oceanic Physics **51** (1), 89–97 (2015).
7. K. R. Helfrich and W. K. Melville, Long nonlinear internal waves, Annual Rev. Fluid Mech. **38**, 395–425 (2006).
8. M. M. Masud, M. Asaduzzaman, and A. A. Mamun, Dust-ion-acoustic Gardner solitons in a dusty plasma with bi-Maxwellian electrons, Physics of Plasmas **19** (10), 103706 (2012).
9. N. N. Rao, P. K. Shukla, and M. Y. Yu, Dust-acoustic waves in dusty plasmas, Planetary and Space Science **38** (4), 543–546 (1990).
10. A. M. Kamchatnov, Y.-H. Kuo, T.-C. Lin, T.-L. Horng, S.-C. Gou, R. Clift, G. A. El, and R. H. J. Grimshaw, Undular bore theory for the Gardner equation, Phys. Rev. E **86** (3), 036605 (2012).
11. M. Wadati, Wave propagation in nonlinear lattice. I, J. Phys. Soc. Japan **38** (3), 673–680 (1975).
12. M. Bokaeeyan, A. Ankiewicz, and N. Akhmediev, Bright and dark rogue internal waves: The Gardner equation approach, Phys. Rev. E **99** (6), 062224 (2019).
13. A. Biswas and E. Zerrad, Soliton perturbation theory for the Gardner equation, Advanced Studies in Theoretical Physics **2** (16), 787–794 (2008).
14. A. M. Wazwaz, Multiple kink solutions for the (2+1)-dimensional integrable Gardner equation, Proc. Romanian Acad. A **15** (3), 241–246 (2014).
15. A. M. Wazwaz, Two (3+1)-dimensional Gardner-type equations with multiple kink solutions, Rom. Rep. Phys. **69**, 108 (2017).
16. K. W. Chow, R. H. J. Grimshaw, and E. Ding, Interactions of breathers and solitons in the extended Korteweg–de Vries equation, Wave Motion **43** (2), 158–166 (2005).
17. Xiao-Yong Wen and Yong Chen, Dynamics of new higher-order rational soliton solutions of the modified Korteweg–de Vries equation, Pramana, **91** (2), 23 (2018).
18. D. E. Pelinovsky and R. H. J. Grimshaw, Structural transformation of eigenvalues for a perturbed

algebraic soliton potential, Phys. Lett. A **229** (3), 165–172 (1997).

19. Zhi-Yuan Sun, Yi-Tian Gao, Ying Liu, and Xin Yu, Soliton management for a variable-coefficient modified Korteweg–de Vries equation, Phys. Rev. E **84** (2), 026606 (2011).
20. A. Ankiewicz and M. Bokaeeyan, Integral relations for rogue wave formations of Gardner equation, Nonl. Dyn. **99**, 2939–2944 (2020).
21. A. Ankiewicz, P. A. Clarkson, and N. Akhmediev, Rogue waves, rational solutions, the patterns of their zeros and integral relations, J. Phys. A: Math. Theor. **43** (12), 122002 (2010).
22. P. A. Clarkson and E. Dowie, Rational solutions of the Boussinesq equation and applications to rogue waves, Transactions of Mathematics and its Applications **1** (1), 1–26 (2017).
23. A. Ankiewicz, A. P. Bassom, P. A. Clarkson, and E. Dowie, Conservation laws and integral relations for the Boussinesq equation, Stud. Appl. Math. **139** (1), 104–128 (2017).
24. Tin Lok Chiu, Tian Yang Liu, Hiu Ning Chan, and Kwok Wing Chow, The dynamics and evolution of poles and rogue waves for nonlinear Schrödinger equations, Commun. Theor. Phys. **68** (3), 290 (2017).
25. R. Hirota, *The direct method in soliton theory*, Cambridge Tracts in Mathematics, vol. 155, Cambridge University Press, Cambridge, 2004.
26. A. Ankiewicz and N. Akhmediev, Multi-rogue waves and triangular numbers, Rom. Rep. Phys. **69**, 104 (2017).
27. A. Ankiewicz and N. Akhmediev, Rogue wave-type solutions of the mKdV equation and their relation to known NLSE rogue wave solutions, Nonl. Dyn. **91** (3), 1931–1938 (2018).
28. A. Ankiewicz, M. Bokaeeyan, and N. Akhmediev, Shallow-water rogue waves: An approach based on complex solutions of the Korteweg–de Vries equation, Phys. Rev. E **99** (5), 050201 (2019).
29. T. Y. Liu, T. L. Chiu, P. A. Clarkson, and K. W. Chow, A connection between the maximum displacements of rogue waves and the dynamics of poles in the complex plane, Chaos **27** (9), 091103 (2017).